from Fig. 3 that the change in the effective refractive index has a power-law dependence on UV fluence. It shows distinctly different behaviours for different dose regions, indicating that there is interplay between at least two different mechanisms of photosensitivity. In the low dose range (<20 J/cm^2), the slope is approximately 0.27 and it is virtually independent of pressure. Beyond a transition region where both mechanisms operate (20–800 J/cm^2), the refractive index change also exhibits power-law dependence. However, in this high-dose region, the slope is pressure dependent, increasing from 0.39 at 26 bar to 0.68 at 160 bar.

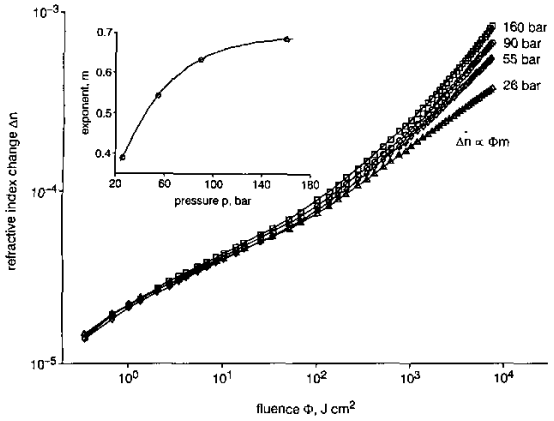

Fig. 3 *Photosensitivity of SMF-28 fibre loaded at different hydrogen pressures*

Inset: Pressure dependence of exponent m at high fluence

Conclusion: We have presented a novel highly accurate technique to measure photosensitivity in optical fibre. Experimental data on photosensitivity measurements of different fibres are presented. The experimental data indicate that two mechanisms of photosensitivity are likely to operate in hydrogen-loaded germanosilicate fibres.

Acknowledgments: The authors acknowledge the financial support for this work by Telkom SA Ltd., ATC (Pty) Ltd., THRIP and RAU, and by CONACYT through the research grant 35460-U.

9 September 2002
Electronics Letters Online No: 20021046
DOI: 10.1049/el:20021046

P.L. Swart and A.A. Chtcherbakov (*Centre for Optical Communications and Sensors, RAU, P.O. Box 524, Auckland Park 2006, South Africa*)

E-mail: pls@ing.rau.ac.za

M.G. Shlyagin and V.V. Spirin (*División de Física Aplicada, CICESE, Apdo. Postal 2732, 22860, Ensenada, B.C., México*)

References

1 OTHONOS, A., and KALLI, K.: 'Fibre Bragg gratings: fundamentals and applications in telecommunications and sensing' (Artech House, Boston, 1999)

2 HILL, K.O., FUJII, Y., JOHNSON, D.C., and KAWASAKI, B.S.: 'Photosensitivity in optical fibre waveguides: application to reflection filter fabrication', *Appl. Phys. Lett.*, 1978, **32**, pp. 647–649

3 DIANOV, E.M., VASILIEV, S.A., FROLOV, A.A., and MEDVEDKOV, O.I.: 'Germanosilicate glass refractive index change under singlet and triplet excitation of germanium oxygen deficient centers', *OSA Tech. Dig. Ser., Bragg Gratings, Photosensitivity, Poling in Glass Fibres Waveguides.*, 1997, **17**, pp. 175–177

4 CANNING, J., and CARTER, A.L.G.: 'Modal interferometer for in situ measurements of induced core index change in optical fibres', *Opt. Lett.*, 1997, **22**, pp. 561–563

5 GARCIA, F.C., and KASHYAP, R.: 'High sensitivity non-birefringent Mach-Zender interferometer for sensing UV induced refractive index change using a unique short Bi-moded optical fibre' *in* ERDOGAN, T., FRIEBELE, E.J., KASHYAP, R. (Eds.): OSA Trends Opt. Photonics, Bragg Gratings, Photosensitivity, Poling in Glass Waveguides, *2000, 33*, pp. 54–60

6 BRINKMEYER, E., JOHLEN, D., KNAPPE, F., and RENER, H.: 'Methods for experimental characterization of UV-written gratings and waveguides' *in* ERDOGAN, T., FRIEBELE, E.J., KASHYAP, R. (Eds.): OSA Trends Opt. Photonics, Bragg Gratings, Photosensitivity, Poling in Glass Waveguides, *2000, 33*, pp. 155–175

7 FOKINE, M., and MARGULIS, W.: 'Large increase in photosensitivity through massive hydroxyl formation' *in* ERDOGAN, T., FRIEBELE, E.J., KASHYAP, R. (Eds.): OSA Trends Opt. Photonics, Bragg Gratings, Photosensitivity, Poling in Glass Waveguides, *2000, 33*, pp. 260–262

8 MIRIDONOV, S.V., SHLYAGIN, M.G., and TENTORI, D.: 'Twin-grating fibre optic sensor demodulation', *Opt. Commun.*, 2001, **191**, (ER3–6), pp. 253–262

Self-healing fibre grating sensor system using tunable multiport fibre laser scheme for intensity and wavelength division multiplexing

Peng-Chun Peng, Hong-Yih Tseng and Sien Chi

A fibre grating sensor system using a tunable multiport fibre laser scheme for intensity and wavelength division multiplexing is proposed. The power ratio (1:2:3) between each output port is used to address the sensing information. The network survivability is also considered. This fibre grating sensor system can enhance the sensing capacity and reliability.

Introduction: Fibre Bragg grating (FBG) sensors have attracted considerable interest because of their applications for quasi-distributed sensing in a smart structure [1]. One of the distinctive advantages provided by FBGs in a sensor system is the multiplexing capability. Several FBG multiplexing techniques have been developed, including wavelength division multiplexing (WDM), time division multiplexing (TDM), spatial division multiplexing (SDM), code division multiplexing access (CDMA), and their combinations [1–4]. The WDM technique incorporated with hybrid star-bus topology or double-bus topology for an FBG sensor has been investigated [5–6]. Such research associated with network survivability would be an ongoing challenge for the practical applications of FBG sensor systems. The survivable network architectures for an FBG sensor system should be cost-effective, crosstalk-free, and output-reliable. Therefore, the capacity of a sensor network should be easily extended and the sensing accuracy should be sufficiently reliable against the noisy environments. Such performance should be considered not only for the optical network layout but also for the electronic signal processing approach.

In this Letter, we propose a self-healing FBG sensor system using a tunable multiport fibre laser scheme for intensity and wavelength division multiplexing. The proposed system can easily enhance the capacity of the sensing FBGs. To maintain the real-time monitoring and indicate the breakpoint position when a fibre link suddenly breaks, a simple self-healing function is also considered in the ring topology of each sensing FBG chain. These advantages can facilitate the remote sensing with high reliability in a smart structure.

Principle: Fig. 1 is a schematic diagram showing the proposed self-healing FBG sensor system. The light source of this sensor system is a tunable fibre ring laser with a Fabry-Perot (F-P) filter for wavelength selection. For WDM incoporated with intensity multiplexing, the output terminal of this fibre laser is a 2×4 coupler comprising three fibre couplers with different coupling ratios. Because of this novel arrangement, three lasing lights with indentical wavelength but different output power emerge from the ring laser simultaneously. The output ratio between the different lasing branches can be designed according to the coupling ratios of the three fibre couplers. The lasing light from each output port is launched into a branch of sensing FBG chain. In contrast with [7], all the sensing FBGs in three chains can have the approximately equal peak reflectivity and need not be fabricated for specified peak reflectivity for intensity multiplexing. Consequently, the proposed multiport fibre laser can easily enhance the capacity of an FBG sensor system by using the intensity multiplexing and WDM technique.

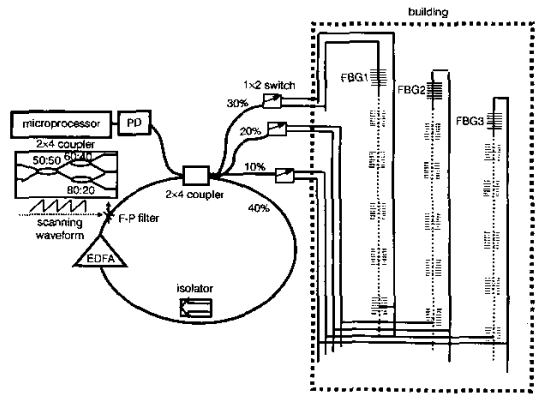

Fig. 1 *Proposed configuration of self-healing fibre grating sensor system using tunable multiport fibre laser scheme for intensity and wavelength division multiplexing*

Experiment: The multiport fibre laser was constructed by an isolator, a 2×4 coupler, a F-P filter with a 35 nm free spectral range (FSR) and ~0.3 nm bandwidth, and a 980 nm laser diode pumping a piece of Er^{+}-fibre through a 980/1550 WDM coupler. The 2×4 fibre coupler comprised a 2×2 fibre coupler (50:50), 1×2 coupler (40:60), and 1×2 coupler (80:20). To enhance the reliability of multipoint sensing, we used self-healing ring architecture by adding a 1×2 optical switch in each sensing branch. The lasing light then travelled through the 2×4 fibre coupler and split into three FBG branches (FBG1 at 1559.70 nm, FBG2 at 1558.74 nm, FBG3 at 1557.23 nm) for experimental demonstration of our proposed multiplexing technique. Because of the 2×4 coupler, the power ratio launched into FBG1, FBG2, and FBG3 was 30%:20%:10%. The peak reflectivity of each FBG was over 99.5%. The backreflected light from each FBG finally propagated through the 2×4 coupler and into the photodetector (PD). The output signal from each PD was fed into a microprocessor to accurately calculate the backreflected wavelength by using the electronic time-counting approach [8].

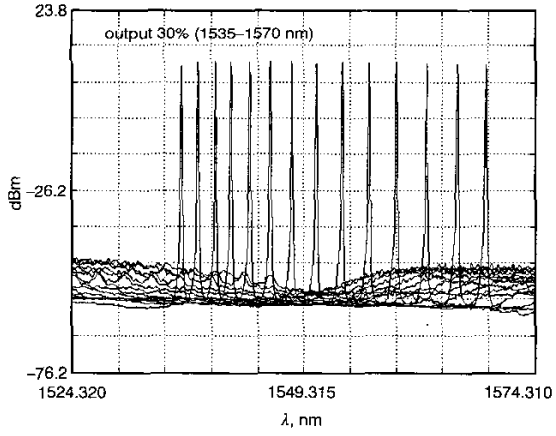

Fig. 2 *Output spectra at 30% lasing port within working range from 1535 to 1570 nm*

Fig. 2 shows the output from the 30% lasing port when we turned the F-P filter using a voltage controller from 0 to 12 V. This operating voltage range can select the lasing wavelength within the working range from 1535 to 1570 nm. The average peak power emerging from this 30% lasing port is 9.25 dBm. For quasi-static strain sensing, we drove the F-P filter using a scanning sawtooth waveform to sweep the wavelength range of the sensing FBGs. Fig. 3 shows the output signal from the PD under the scanning F-P operation. Obviously, by using electronic comparators, this output signal can easily be normalised by the magnitude of the maximum peak intensity (FBG1). Because of this intensity multiplexing, the strain measurement can be achieved using the electronic time-counting signal processing. Furthermore, the microprocessor can control the 1×2 switch in each branch of the ring architecture to check the breakpoint occurring in the fibre sensor network. Such a simple self-healing function in this ring topology can maintain the real-time monitoring and indicate the breakpoint position when the fibre link suddenly breaks. Finally, in contrast with the broadband source adopted in [7] for intensity multiplexing and WDM, the light source of our proposed sensor system is a fibre ring laser, which can enhance the optical signal-to-noise ratio (OSNR) and the sensing resolution for the system. These advantages facilitate the accurate measurement that is sufficiently reliable against the noisy environments, especially for the long-distance remote sensing in a smart structure.

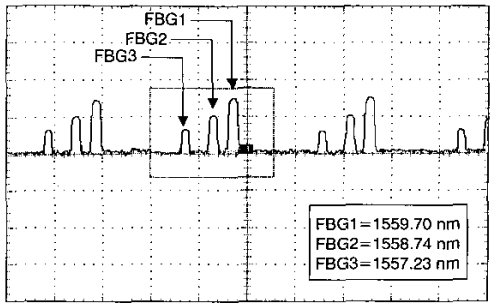

Fig. 3 *Output signal from PD under scanning F-P filter operation*
Horizontal scale: 5 ms/div.; vertical scale: 500 mV/div.

Conclusion: A self-healing FBG sensor system using a tunable multiport fibre laser scheme for WDM incorporated with intensity division multiplexing has been proposed and experimentally demonstrated. Such a multiplexing technique can easily increase the capacity of the FBG sensor system. The network survivability of this proposed FBG sensor is also considered by adding a switch in the ring architecture. In the experiment, a three-point sensor system was shown. The experimental results show that the tunable multiport fibre laser for intensity multiplexing and WDM can enhance the OSNR and resolution of the sensor system. These advantages facilitate the electronic signal processing for a FBG sensor system and lead to a simple fibre sensor network with a large number of FBG sensing applications.

17 May 2002
Electronics Letters Online No: 20021016
DOI: 10.1049/el:20021016

Peng-Chun Peng, Hong-Yih Tseng and Sien Chi (*Institute of Electro-Optical Engineering, National Chiao-Tung University, 1001 Ta Hsueh Road, Hsinchu, Taiwan, 300, Republic of China*)

E-mail: pcpeng.eo90g@nctu.edu.tw

References

1 KERSEY, A.D., DAVIS, M.A., PARTRICK, H.J., LEBLANC, M., KOO, K.P., ASKINS, C.G., PUTNAM, M.A., and FRIEBELE, E.J.: 'Fiber grating sensors', *J. Lightwave Technol.*, 1997, **15**, pp. 1442–1463

2 YU, Y., LUI, L., TAM, H., and CHUNG, W.: 'Fiber-laser-based wavelength-division multiplexed fiber Bragg grating sensor system', *IEEE Photonics Technol. Lett.*, 2001, **13**, pp. 702–704

3 CHAN, C.C., JIN, W., HO, H.L., and SULEYMAN DEMOKAN, M.: 'Performance analysis of a time-division-multiplexed fiber Bragg grating sensor array by use of a tunable laser source', *IEEE J. Sel. Top. Quantum Electron.*, 2000, **6**, pp. 741–749

4 KOO, K.P., TVETEN, A.B., and VOHRA, S.T.: 'Dense wavelength division multiplexing of fibre Bragg grating sensors using CDMA', *Electron. Lett.*, 1999, **35**, pp. 165–167

5 MONTOYA, V., LOPEZ-AMO, M., and ABAD, S.: 'Improved double-fiber-bus with distributed optical amplification for wavelength-division multiplexing of photonic sensors', *IEEE Photonics Technol. Lett.*, 2000, **12**, pp. 1270–1272

6 ACHAERANDIO, E., JARABO, S., ABAD, S., and LOPEZ-AMO, M.: 'New WDM amplified network for optical sensor multiplexing', *IEEE Photonics Technol. Lett.*, 1999, **11**, pp. 1644–1646

7 ZHANG, L., LIU, Y., WILIAMS, J.A.R., and BENNION, I.: 'Enhanced FBG strain sensing multiplexing capacity using combination of intensity and

wavelength dual-coding technique', *IEEE Photonics Technol. Lett.*, 1999, **11**, pp. 1638–1641

8 SZPLET, R., KALISZ, J., and SZYMANOWSKI, R.: 'Interpolating time counter with 100 ps resolution on a single FPGA device', *IEEE Trans. Instrum. Meas.*, 2000, **49**, pp. 879–883

Image fragile watermarking based on fusion of multi-resolution tamper detection

Junquan Hu, Jiwu Huang, Daren Huang and Yun Q. Shi

A new discrete wavelet transform-based image fragile watermarking scheme exploiting the features of the human visual system is presented. Fusion of multi-resolution tamper detections, and mathematical morphology operations are developed for accurate tamper detection. As a result, malicious tamper and the tampered regions can be detected, while toleration towards high quality lossy image compression is achieved.

Introduction: Fragile watermarking plays an important role in image authentication [1, 2]. It is required that fragile watermarking should be able to detect malicious modifications effectively yet tolerate mild modifications such as commonly used JPEG compression. In this Letter, we propose a new semi-fragile watermark scheme in discrete wavelet transform (DWT) domain aiming at better performance.

Watermark embedding: In our work, watermark is a binary logo. For multi-resolution tamper detection and embedding convenience, a pyramid structure of the binary logo is constructed by applying the resolution reduction (RR) procedure adopted by JBIG [3]. The data in the pyramid are then embedded into LL_3, HH_2, and HH_1 sub-bands of the host image in the L-level DWT domain. According to the requirements of invisibility and tolerance towards lossy compression, the data are embedded into the low frequency and high frequency sub-bands. To embed, the L-level DWT is applied firstly to the original image. Then, for a specific sub-band, we calculate

$$Q_{i,j} = \begin{cases} 0 & \lfloor f(i,j)/JND(i,j) \rfloor \quad \text{is even} \\ 1 & \lfloor f(i,j)/JND(i,j) \rfloor \quad \text{is odd} \end{cases} \tag{1}$$

where $f(i, j)$ denotes a DWT coefficient's magnitude, $JND(\cdot)$ element in the corresponding Watson's quantisation matrix [4], $\lfloor \cdot \rfloor$ the floor function. We adopt Watson's quantisation matrix because it has taken into consideration the features of the human visual system (HVS). Define $s = \lfloor f(i, j)/JND(i, j) \rfloor$. To a pre-specified m, we divide the interval $[sJND(i, j), (s + 1)JND(i, j)]$ into 2^{m-1} equal parts, and denote the length of each part as *length*. The ordinal number of the part in which a coefficient is located is denoted as $t \in [1, 2, 3, \ldots, 2^{m-1}]$. We embed m bits of the mark data at once, and denote the first bit by $w(i, j)$, the remaining $m - 1$ bits by r in decimal scale with $r \in [0, 1, 2, \ldots, 2^{m-1} - 1)$. The main idea is to limit the modification of the DWT coefficients during the data embedding within one $JND(\cdot)$ in order to make the distortion generated in data hiding less noticeable. The specific rule for coefficient alteration is as follows:

$$\tilde{f}(i,j) = \begin{cases} JND(i,j) \cdot s + (r + 0.5) \cdot length & \text{if } Q_{i,j} = w(i,j) \\ f_2 & \text{if } Q_{i,j} \neq w(i,j) \end{cases} \tag{2}$$

where

$$f_2 = \begin{cases} JND(i,j) \cdot (s+1) + (r + 0.5) \cdot length \\ \quad \text{if } (t = r + 1 \text{ and } length/2 < f(i,j) - \\ \quad JND(i,j) \cdot s - r \cdot length) \text{ or } t > (r + 1) \\ JND(i,j) \cdot (s-1) + (r + 0.5) \cdot length \\ \quad \text{if } (t = r + 1 \text{ and } length/2 > f(i,j) - \\ \quad JND(i,j) \cdot s - r \cdot length) \text{ or } t < (r + 1) \end{cases} \tag{3}$$

Watermark extraction: In the watermark retrieval, the L-level DWT is applied to the possible watermarked image. Denote the DWT coefficients as $f'(i, j)$. Similar to the Q_{ij}, s and ordinal number t used in the embedding procedure, Q'_{ij}, s' and t' are calculated according to the same rule with $f(i, j)$ replaced by $f'(i, j)$. Hence, the extracted watermark is:

$$w = Q'_{i,j} \cdot 2^{m-1} + t' \tag{4}$$

We can then obtain m bits of the extracted mark simply by transforming w to binary scale.

Tamper detection: We have estimated the scheme's fragility, and found that the variable m is important to fragility. As m increases, the scheme becomes more and more sensitive to image modification. Hence, m is chosen as 4 in our work in order to achieve both tamper detection capability and tolerance towards mild modification simultaneously. In tamper detection, we generate a set of binary difference images between the marking logo image and the extracted candidate logo image in different resolutions, where binary 1 represents an error pixel, while binary 0 no error. To a specific resolution, mathematical morphology operations are applied to remove noise-like pixels and to create a compact tamper region in the difference image. Specifically, a dilation operation is applied firstly to create compact regions, then an erosion operation is applied in succession to remove the noise-like error pixel, and finally another dilation operation is applied to restore the original size of the compact regions. The structure element used in each operation is calculated carefully using order statistics [5]. We further define error detection ratio λ_l and error dense ratio δ_l of the difference image in a specific resolution level l as follows:

$$\lambda_l = \frac{\text{card}\{\text{error pixel}\}}{\text{card}\{\text{total pixel}\}}, \qquad \delta_l = \frac{\text{card}\{\text{dense pixel of error detection}\}}{\text{card}\{\text{error pixel}\}} \tag{5}$$

where $\text{card}\{\cdot\}$ denotes the cardinality of the argument set, and a pixel of error detection is dense if there is at least one error detection pixel in its surrounding eight neighbours. Using the above parameters, we define the following rules in authentication. (i) If $\lambda_l = 0$ for every resolution level l, the tested image has been neither maliciously tampered nor incidental distorted. (ii) If there exists some l such that $\lambda_l > 0$ and $\delta_l < \alpha$, where α is a preset threshold, then the tested image has encountered only incidental distortions. In experiments, we set $\alpha = 0.9$. (iii) $\lambda_l > 0$ and $\delta_l \geq \alpha$ for every l, then the tested image has been maliciously tampered.

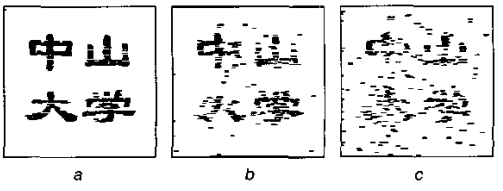

a b c

Fig. 1 *Mark extracted from marked image compressed by JPEG with quality factor*
a 90, *b* 70, *c* 50

Simulation results: Many experiments have been conducted to demonstrate the effectiveness of tamper detection with the proposed scheme. The test results on 'Lena' and 'Baboon' images, both of $256 \times 256 \times 8$ bits, are reported here. The peak signal-to-noise ratios (PSNR) of the watermarked images are 38.43 and 31.86 dB, respectively. It is noted that the PSNR is only 34.26 dB for Lena with the scheme in [2]. This 4.17 dB increase in PSNR is due to the utilisation of Watson's quantisation matrix. Fig. 1 shows the extracted watermarks from the marked image corrupted by JPEG compression at the different quality factors. Obviously, when the quality factor is higher than 50%, we can discern the content of the mark, but this is not true when the quality is equal to or lower than 50%. Hence, the case with quality factor lower than 50% shall be judged as serious distortion. Fig. 2 shows that our scheme is fragile to partial replacement attack. The detection results show clearly that tamper has occurred and the tamper region has been located. To illustrate the effectiveness of the proposed scheme, we compare its performance with that reported in [2]. In [2], only the detection results at the various resolution levels are listed. When the detection results from different resolutions are different, there is no specific rule available that makes a decision. The parameter used to judge whether an image is tampered or not, named